

Semiclassical study of the isomerization states of HCP

Marc Joyeux^{a)} and Dominique Sugny

Laboratoire de Spectrométrie Physique (CNRS UMR 5588), Université Joseph Fourier-Grenoble I, BP 87, F-38402 St Martin d'Hères, France

Vivian Tyng and Michael E. Kellman

Department of Chemistry, University of Oregon, Eugene, Oregon 97403

Haruki Ishikawa

Department of Chemistry, Graduate School of Science, Tohoku University, Aoba-ku, Sendai 980-77, Japan

Robert W. Field

Department of Chemistry, Massachusetts Institute of Technology, Cambridge, Massachusetts 02139

Christian Beck and Reinhard Schinke

Max-Planck-Institut für Strömungsforschung, D-37073 Göttingen, Germany

(Received 15 October 1999; accepted 8 December 1999)

The vibrational spectrum of HCP (phosphaethyne) is studied and analyzed in terms of a 1:2 resonance effective Hamiltonian. The parameters of the model Hamiltonian are determined by fitting 361 out of the first 370 energy levels obtained from diagonalization of the full Hamiltonian, which is based on a newly calculated potential-energy surface with near spectroscopic accuracy. It is demonstrated that all features characteristic of the approach to the HCP \leftrightarrow CPH isomerization, such as the strong mixing between the bending and CP-stretching motions, the appearance of “isomerization states” (large amplitude bending motion) at intermediate energies, and the diagnostically significant appearance of a zig-zag pattern in the energy spacings between neighboring levels within each polyad, are quantitatively reproduced by the effective Hamiltonian. The semiclassical analysis of the model Hamiltonian for specific combinations of the HC-stretch and polyad quantum numbers explains all of the observed features of the full Hamiltonian in terms of stable and unstable periodic orbits. In particular, the birth of the isomerization states is found to be related to a saddle-node bifurcation of the classical phase space. The connection with the “polyad phase sphere” representation of quantum polyads is also discussed. © 2000 American Institute of Physics. [S0021-9606(00)00809-6]

I. INTRODUCTION

The potential-energy surface (PES) of phosphaethyne (HCP) in its ground electronic state has received much attention in the last few years, both from the experimental¹⁻⁵ and theoretical^{1,6-9} points of view. The reason is that some unusual features observed in the stimulated emission pumping (SEP) spectra at about 20 000 cm⁻¹ above the ground state³⁻⁵ might well be signatures for the isomerization process leading from HCP to CPH. Indeed, the calculations^{6,7,9} have shown the existence of two distinct families of bending states: One with wave functions confined to small bending angles and the other one sampling all of the isomerization pathway from HCP to CPH. The members of this later family are called “isomerization” states in order to distinguish them from the “normal” states belonging to the first family. The family of normal states starts at low energies and persists well above the isomerization saddle at about 24 400 cm⁻¹ above the ground state. In contrast, the family of isomerization states starts abruptly at intermediate energies (about 15 000 cm⁻¹ above the ground state) and can be followed up to the isomerization saddle. In agreement with

classical and semiclassical theories, it was pointed out^{6,7,9} that the appearance of the isomerization states is associated with a saddle node (SN) bifurcation of the periodic orbits (POs) of the classical Hamiltonian, which is due to the Fermi resonance between the bending and the CP stretching motions⁹ and takes place at 13 800 cm⁻¹ above the quantum ground state. When plotted on the same diagram, isomerization states are seen to lie exactly on top of the family of stable POs born at this bifurcation, both of them following closely the isomerization pathway.

It was furthermore shown in Ref. 9 that all the details observed in the quantum spectrum do have a dynamical content, and that this content is most readily understood through the semiclassical analysis of an effective resonance Hamiltonian with parameters obtained by fitting the quantum spectrum. It is only through the gathering of all the different pieces—namely (i) a large amount of experimental data, (ii) exact calculation on an *ab initio* PES, (iii) the study of the classical phase space for the *ab initio* PES, and (iv) the semiclassical study of the effective Hamiltonian—that a precise understanding of the highly excited vibrational dynamics of HCP is possible.

The above mentioned work on the isomerization states of HCP and their connection with a classical bifurcation,^{6,7,9}

^{a)}Electronic mail: marc.joyeux@ujf-grenoble.fr

however, relies on a preliminary PES,⁷ which, although qualitatively correct, is not sufficiently precise for quantitative predictions and direct comparison with experiments. Since the publication of Ref. 7, Schinke and co-workers have constructed a completely new surface, the details of which are given in Ref. 10. The fundamental frequencies calculated from this new surface now agree to better than 4 cm⁻¹ with the observed ones and the overtone and combination frequencies to better than 20 cm⁻¹ up to 20 000 cm⁻¹ above the zero-point energy. The study of the classical phase space using this surface confirms that a classical bifurcation coincides with the appearance of isomerization states.^{10,11} However, many quantum features differ substantially from those observed in the first PES, as can be checked from a comparison between Refs. 6, 7, and 9 on one side and Refs. 10 and 11 and the present article on the other side. The dynamics is, therefore, expected to be also very different. Owing to the fact that HCP is so far an almost unique system in the study of isomerization, because of the considerable amount of experimental data and the (now) accurate global PES, it was felt that a semiclassical study dealing with the new surface was worthwhile, in order to obtain a complete and coherent description of this prototypical molecule.

This article is organized as follows: A brief description of the Fermi resonance effective Hamiltonian, which will be used throughout the paper, is presented in Sec. II. Section III contains a recount of the features observed in the exact quantum spectrum and which are closely reproduced by the resonance Hamiltonian. It will be the goal of the remainder of the article to extract the dynamical information contained in these features through the semiclassical study of the resonance Hamiltonian: The birth and gradual arrangement of isomerization states along the isomerization pathway are first discussed in Sec. IV in terms of classical *stable* periodic orbits. Then, quantizing trajectories are analyzed in Sec. V, in order to understand the interleaving of isomerization and normal states at the bottom (i.e., low-energy region) of quantum polyads. At last, the patterns in the energy spacings between neighboring levels, which are most useful to experimentalists, are discussed in Sec. VI in terms of the classical *unstable* periodic orbits.

II. THE FERMI RESONANCE HAMILTONIAN

The explicit matrix elements for the Fermi resonance Hamiltonian H in the basis of harmonic-oscillator products (nondegenerate for modes 1 and 3, doubly degenerate for mode 2) are taken to be, respectively

$$\begin{aligned} \langle v_1, v_2, v_3 | H | v_1, v_2, v_3 \rangle = & \sum_i \omega_i n_i + \sum_{i \leq j} x_{ij} n_i n_j \\ & + y_{222} n_2^3 + z_{2222} n_2^4, \\ n_1 = v_1 + \frac{1}{2}, \quad n_2 = v_2 + 1, \quad n_3 = v_3 + \frac{1}{2}, \end{aligned} \quad (2.1)$$

for the Dunham diagonal expansion and:

$$\begin{aligned} \langle v_1, v_2, v_3 | H | v_1, v_2 + 2, v_3 - 1 \rangle = & -n_2 n_3^{1/2} \left(k + \sum_i k_i n_i \right), \\ n_1 = v_1 + \frac{1}{2}, \quad n_2 = v_2 + 2, \quad n_3 = v_3, \end{aligned} \quad (2.2)$$

TABLE I. The fitted molecular constants of HCP in Eqs. (2.1), (2.2), and (2.4) and the corresponding uncertainties (one times the standard deviation).

Parameter	Value (cm ⁻¹)	Uncertainty (cm ⁻¹)
ω_1	3343.1225	1.6852
ω_2	697.7797	0.7516
ω_3	1301.0838	0.6911
x_{11}	-55.0161	0.2892
x_{12}	-16.8174	0.1186
x_{13}	-4.3375	0.1838
x_{22}	-5.3477	0.0829
x_{23}	-4.6460	0.0439
x_{33}	-5.8619	0.0541
y_{222}	0.233 45	0.005 20
z_{2222}	-0.005 62	0.000 14
k	3.6115	0.1585
k_1	0.805 60	0.043 76
k_2	0.067 27	0.008 45
k_3	-0.220 67	0.010 97

for the off diagonal Fermi coupling. Unlike in Refs. 8 and 9, the convention of spectroscopists¹⁻⁵ is used here for labeling the normal modes, i.e., indexes 1, 2, and 3 refer respectively to the CH stretch, the bend and the CP stretch. The vibrational angular momentum ℓ , which results from the degeneracy of the bending motion, is assumed to be zero in Eqs. (2.1) and (2.2), as was done in the previous theoretical works on HCP where only the nonrotating molecule ($J=0$) was studied.^{6,7,9} Without this assumption, slightly more complex expressions must be used.^{12,13} The fifteen parameters: Three ω , six x , one y , one z , and four k were fitted against 361 out of the first 370 levels obtained from exact quantum calculations on the new PES.¹⁰ These levels have up to 30 quanta in the bending degree of freedom and 6 quanta in the CH stretch. Numerical values for the parameters can be found in Table I. The rms error for the 361 levels is 7.7 cm⁻¹ and the maximum error 35.6 cm⁻¹.

The Fermi resonance in Eq. (2.2) destroys one good quantum number, so that there remain only two good quantum numbers in addition to the vibrational angular momentum ℓ . These are the number, v_1 , of quanta in the CH stretch and the so-called polyad number, P , where

$$P = v_2 + 2v_3. \quad (2.3)$$

The Fermi resonance only couples levels of the basis of harmonic-oscillator products with the same values of v_1 and P . For even values of P , there are $(P/2) + 1$ levels with the same values for v_1 and P . Such a subset of levels is called a polyad and will be denoted $[v_1, P]$, as in Refs. 5 and 11. Individual levels can be further characterized by their position i inside the polyad. The convention that $i=0$ at the top of the polyad and $i=P/2$ at the bottom is used throughout this article, as in Refs. 5 and 11.

Let us finally mention that the resonance Hamiltonian, in addition to energy values, is also able to reproduce with great accuracy the features observed in the *ab initio* wave functions. For example, the wave functions for the 12 states of polyad $[v_1, P] = [0, 22]$ are plotted in Fig. 1 for the resonance Hamiltonian. The basis functions are taken again as harmonic-oscillator products (a doubly degenerate oscillator

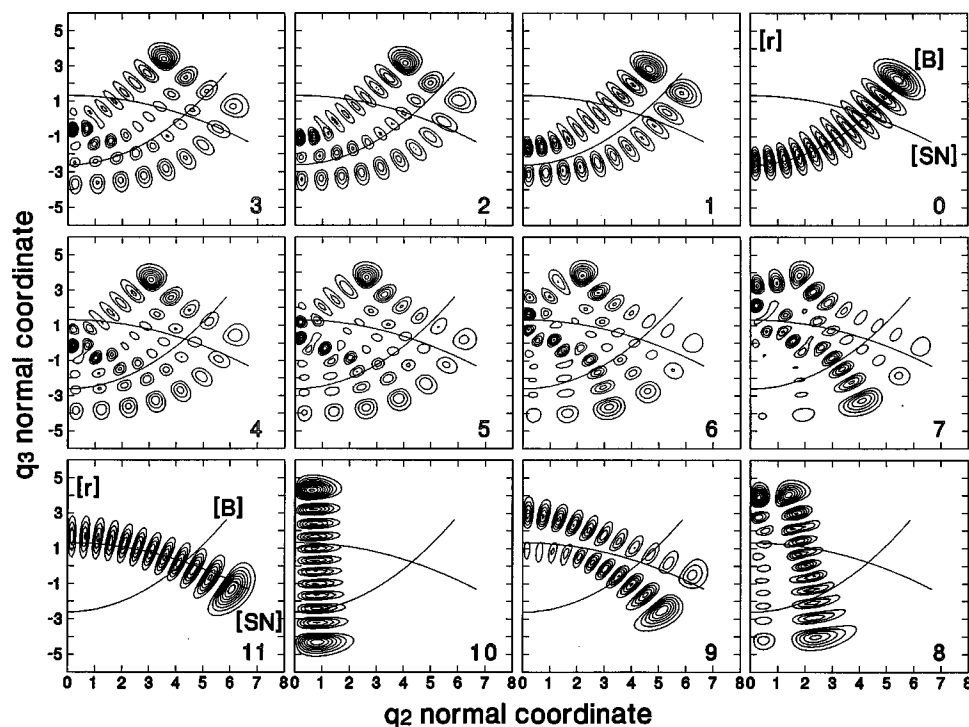


FIG. 1. Plot in the (q_2, q_3) plane of the wave functions of the 12 levels, which belong to polyad $[v_1, P]=[0, 22]$. The horizontal axis q_2 (bend) ranges from 0 to 8 and the vertical axis q_3 (CP stretch) from -6 to 6 . This polyad spans the energy range from $13\,425$ to $13\,948\text{ cm}^{-1}$ above the ground state. The three stable periodic orbits $[r]$, $[B]$, and $[SN]$ are also plotted ($[r]$ merges into the vertical q_3 axis and cannot be clearly distinguished). Note the coincidence of eigenstates 0, 10, and 11 with orbits $[B]$, $[r]$, and $[SN]$, respectively.

is taken for the bending degree of freedom). This figure compares very well with Fig. 10 of Ref. 11, which shows some wave functions for the new PES. On the other hand, the expression for the classical Hamiltonian can be written in the form

$$H = \sum_i \omega_i I_i + \sum_{i \leq j} x_{ij} I_i I_j + y_{222} I_2^3 + z_{2222} I_2^4 + 2I_2 I_3^{1/2} \cos(2\varphi_2 - \varphi_3) \left(k + \sum_i k_i I_i \right). \quad (2.4)$$

The (I_k, φ_k) are action-anglelike sets of conjugate coordinates, such that

$$q_k = \sqrt{2I_k} \cos \varphi_k, \\ p_k = -\sqrt{2I_k} \sin \varphi_k \quad (1 \leq k \leq 3). \quad (2.5)$$

The classical study is greatly simplified when Eq. (2.4) is expressed in terms of I_1 and of new conjugate variables (I, θ) and (J, ψ) obtained from (I_2, φ_2) and (I_3, φ_3) through the following canonical transformation:

$$I = I_2 + 2I_3, \\ J = 2I_3, \\ \theta = \varphi_2, \\ \psi = \frac{\varphi_3}{2} - \varphi_2. \quad (2.6)$$

Inserting the transformations of Eq. (2.6) into Eq. (2.4), the nonlinear coupling becomes $(I-J)J^{1/2} \cos(2\psi)(K + K_1 I_1 + K_2 I$

$+K_3 J)$, with trivial, linear relations between the parameters k and k_i of Eq. (2.4) and the parameters K and K_i . The important point is that this coupling does not depend on the angles φ_1 and θ , which implies that I_1 and I are constants of motion. It is now well understood^{14,15} that their values are also action integrals of the system and that the Einstein–Brillouin–Keller (EBK) quantization rules¹⁶ dealing with these two action integrals are

$$I_1 = v_1 + \frac{1}{2} \\ I = P + 2. \quad (2.7)$$

In other words, each level belonging to the polyad $[v_1, P]$ is associated with a semiclassical quantizing trajectory with constants of motion I_1 and I equal, respectively, to $v_1 + 1/2$ and $P + 2$. Examples of these trajectories will be seen below in the phase space portraits of Figs. 5 and 6 and in the essentially equivalent polyad phase sphere representation in Fig. 7(a). The third action integral of the system, which will be called \mathcal{J} , can be obtained by computing a simple integral derived from the expression of energy in coordinates (I_1, φ_1) , (I, θ) , and (J, ψ) [see Eqs. (2.13) and (2.14) in Ref. 9]. The third EBK quantization rule then states that the quantizing trajectories are those which satisfy Eq. (2.7) and for which, in addition, \mathcal{J} is half-integral (positive or negative). An alternate way to find quantizing trajectories corresponding to the quantum energy levels, without numerical propagation, is to solve directly by quadrature for the classical trajectories that have the same energy as the quantum levels of the spectroscopic Hamiltonian. This approach has been explored extensively by Kellman and co-workers.^{17–24} The

correspondence between classical and quantum mechanics ensures that this is a good approximation, at least not too close to separatrices. In this study, the difference in energy between levels obtained in the two approaches is not larger than 1.3 cm^{-1} for polyad $[v_1, P] = [0, 22]$. It should be noted that in the work of Kellman *et al.*,^{17–19, 21–24} the phase space description involves a spherical surface, the “polyad phase sphere.” The phase sphere description is completely equivalent to the one described above, when it is realized that one goes from one to the other simply by transforming from a cylindrical, or Mercator representation, to an equivalent representation on the sphere. The phase sphere representation is displayed in Fig. 7 below with more detail about its topological properties.

III. THE FEATURES OBSERVED IN THE QUANTUM SPECTRUM

The principal features, which are evident in the plots of the wave functions obtained from the new surface,^{10,11} are recounted in this section, before the dynamical content is extracted in the next three sections.

For the polyads with $v_1 = 0$ the wave functions show the usual, low P -behavior up to $P = 14$: They evolve regularly from a wave function with $P/2$ nodes along a line almost parallel to the q_3 axis (the CP stretch coordinate) at the bottom of the polyads to another wave function with $P/2$ nodes along another line approximately parallel to the q_2 axis (the bend coordinate) at the top of the polyads. In contrast, states with qualitatively different wave functions have definitely come into existence at $P = 18$ (see Fig. 10 of Ref. 11). The first state with a clearly new wave function is the second lowest one ($i = P/2 - 1 = 8$) in this polyad and is located at $11\,159 \text{ cm}^{-1}$ above the ground state. This new class of wave functions still contains a significant contribution of CP-stretch, which however decreases steadily with increasing polyad number. Above polyad $P = 22$, the new wave functions are almost pure bend and closely follow the minimum energy path leading from HCP to CPH. A second isomerization state appears in the same polyad $P = 22$; the two isomerization states are the lowest ($i = P/2 = 11$) and the third lowest one ($i = P/2 - 2 = 9$) in the polyad, while the second lowest one ($i = P/2 - 1 = 10$) displays motion along the CP stretching coordinate. These features are closely reproduced by the resonance effective Hamiltonian, as can be verified in Fig. 1. The number of isomerization states continues to increase with P and there are readily five of them in polyad $P = 32$, which have respective positions $i = 16, 15, 14, 13$, and 11. The level with $i = 12$, which is located between two isomerization states, is again a pure CP-stretching state. Moreover, in the same energy range above polyad $P = 18$, the plot of the energy gaps between neighboring levels inside a given polyad displays some kind of zig-zag pattern. This pattern differs again markedly from the simple minimum which was observed for the first surface and was shown to be a fingerprint of the classical bifurcation in the quantum spectrum. To conclude this brief summary of the exact quantum calculations, let us mention that for $v_1 = 1$ and $v_1 = 2$ the main features are the same as for $v_1 = 0$, except that the first

appearance of isomerization states happens earlier as a function of P and that the interleaving of isomerization and normal states completely ceases with $v_1 = 2$.

The goal of the remainder of this article is to extract the dynamical information contained in these observations using the formalisms of periodic orbits (POs) and semiclassical quantization. Following the pioneering work of Gutzwiller^{25–27} and Heller,^{28,29} there have been several numerical applications, which have demonstrated the importance of POs in understanding the localization of quantum wave functions, which in turn is helpful for understanding spectral patterns.^{30–33} The key idea is that classical stable POs form the “backbones” of quantum wave functions, or, in other words, that they are approximately parallel to the nodal and antinodal lines of the wave functions. Therefore, a classical bifurcation, that is, a point [here in the (E, I, I_1) space] where the number and/or the stability properties of the POs change abruptly, might be expected to be associated with clear-cut changes in the behavior of the wave functions. In particular, a tangent (or saddle-node) bifurcation corresponds to the simultaneous creation (or destruction) of one stable and one unstable PO, so that families of wave functions with nodal lines oriented along the corresponding stable PO might be expected to appear (or to disappear) at this bifurcation. Moreover, since the CH stretching motion (mode 1) does not participate in the Fermi resonance, the POs for the resonance Hamiltonian of Sec. II need only be searched for in the reduced subspace (p_2, p_3, q_2, q_3) instead of the full six-dimensional space, as was shown in Ref. 9. Procedures for performing the bifurcation analysis for the spectroscopic Hamiltonian are described in detail in earlier works of Joyeux *et al.*,⁹ Jost *et al.*,³⁴ Li *et al.*,²² and Jacobson *et al.*³⁵ and the reader is referred to these articles for more details.

Each one of the next three sections will explore a particular semiclassical feature and derive a different class of information from the quantum spectrum.

IV. STABLE PERIODIC ORBITS AND ISOMERIZATION STATES

Stable POs and bifurcations are discussed in this section, in order to understand why isomerization states appear close to the bottom of the polyads and why their wave functions arrange themselves only gradually along the isomerization pathway, as described in the previous section.

The search for bifurcations gives the total action I as a function of I_1 . Bifurcations, therefore, appear as curves, which divide the (I_1, I) plane into distinct regions, each region being characterized by a different number of POs. Owing to the EBK quantization rules in Eq. (2.7), this bifurcation diagram can be plotted in the (v_1, P) plane in order to enable an easier comparison with the quantum results; however, v_1 and P are allowed to assume continuous real values. Such a plot appears in Fig. 2, where the solid line, representing the SN bifurcation, divides the (I, I_1) plane into two regions, containing two and four periodic orbits, respectively (the dashed line depicts the quantum numbers v_1 and P for the highest polyads included in the fit, and the analysis is, therefore, valid only below this line). In contrast to the cal-

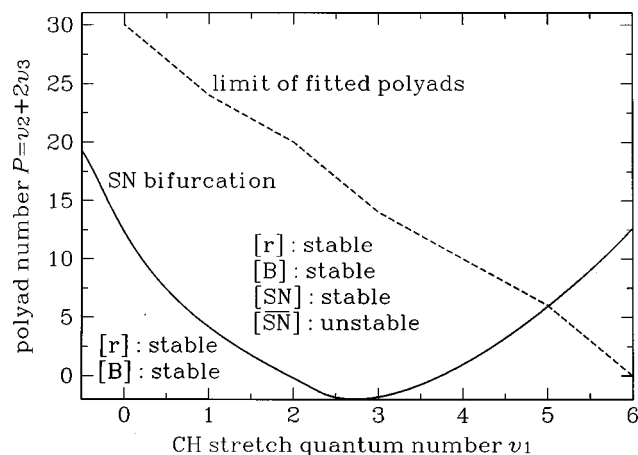


FIG. 2. Plot in the (v_1, P) plane of the bifurcation diagram of the periodic orbits of HCP. The solid line indicates the saddle-node (or tangent) bifurcation. The stable $[SN]$ and the unstable $[SN]$ periodic orbits appear at the bifurcation. The two types of stable periodic orbits, $[r]$ and $[B]$, exist both below and above the bifurcation. The dashed line is the upper energy limit of the fitted polyads and the validity of the analysis can be assured only below this line.

culations with the first PES,^{6,7,9} a single tangent (or saddle-node) bifurcation is found in the range of fitted polyads. The “U” shape of this line can easily be interpreted in terms of the detuning of the zero-order levels from exact Fermi resonance. Indeed, it seems to be a general result that as the zero-order resonance condition (here $2\omega_2 = \omega_3$) is approached more closely, the lower is the polyad number at which the first tangent bifurcation appears. The energy gap between the levels $(v_1, 0, 1)$ and $(v_1, 2, 0)$, computed from the zero-order Dunham expansion alone, is equal to -67.3 , -38.0 , -8.7 , 20.6 , 49.9 , 79.2 , and 108.5 cm^{-1} for v_1 increasing from 0 to 6. Exact resonance therefore occurs somewhere between $v_1 = 2$ and $v_1 = 3$, that is, in the same range of values of v_1 where the bifurcation curve reaches its minimum ($P = -2$).

The search for the SN bifurcation helps to put lower limits to the energy at which isomerization states first appear. Indeed, the SN bifurcation is found at $P = 12.30$ and $E = 7744$ cm^{-1} above the quantum-mechanical ground state for $v_1 = 0$, $P = 4.16$, and $E = 5850$ cm^{-1} for $v_1 = 1$, $P = -0.21$, and $E = 6176$ cm^{-1} for $v_1 = 2$, $P = -1.81$, and $E = 8159$ cm^{-1} for $v_1 = 3$, and $P = 0.98$ and $E = 12840$ cm^{-1} for $v_1 = 4$ (for values of v_1 larger than four, the bifurcation does not occur inside the fitted polyad range so that polyads with $v_1 > 4$ are excluded from our discussion). Negative values of P for $v_1 = 2$ and $v_1 = 3$ mean that the bifurcation has already taken place for the first quantum polyad ($P = 0$). Notice, however, that these numerical values for P are only lower limits for the appearance of isomerization states because P can assume only even integer values in quantum mechanics. Moreover, a zero-point energy argument (to be presented in Sec. V) is responsible for the fact that clear isomerization states first appear for values of P sometimes substantially higher than the value of P at the bifurcation.

More detailed information concerning POs is gained from the plot of their energy and their bend/CP–stretch characteristics. The plot of the energy values of the POs is given

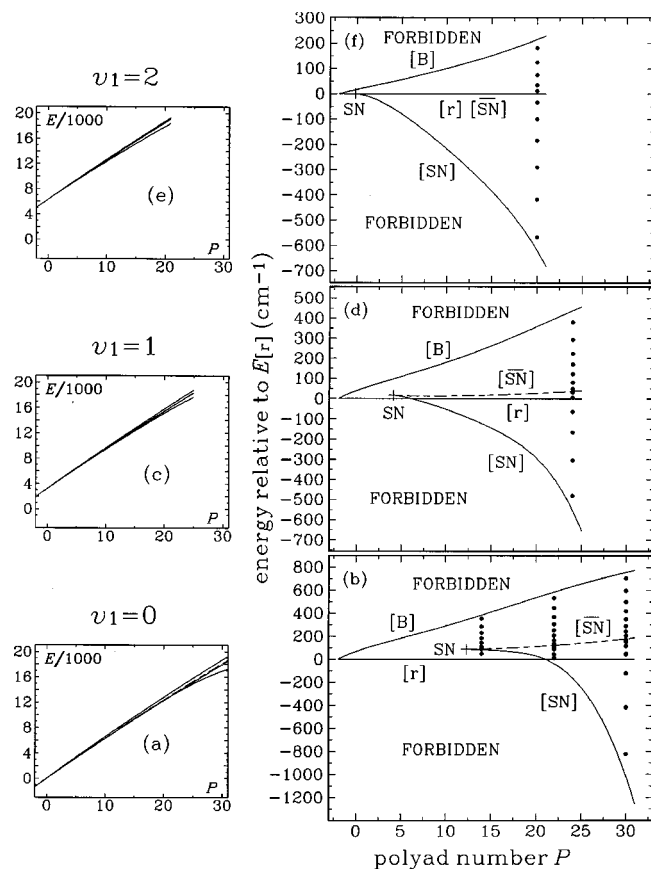


FIG. 3. (left): Plot of the energies of the periodic orbits of HCP relative to the quantum-mechanical ground state as a function of the quantum polyad number P for $v_1 = 0$ (bottom), $v_1 = 1$ (middle) and $v_1 = 2$ (top). Same as in the left column, but with an energy scale expanded around the energy of the stable periodic orbit $[r]$. Solid lines mark the energies of the stable periodic orbits $[r]$, $[B]$, and $[SN]$ and the dashed line shows the energy of the unstable periodic orbit $[SN]$. The cross labeled SN indicates the saddle-node (or tangent) bifurcation at which $[SN]$ and $[SN]$ are created simultaneously. The classically allowed region as well as the energy levels of the quantum polyads always lie between the energies of the two outermost stable periodic orbits. The five columns of dots in the three panels on the right represent the energy levels of the polyads $[v_1, P] = [0, 14]$, $[0, 22]$, $[0, 30]$, $[1, 24]$, and $[2, 20]$.

in Fig. 3 for $v_1 = 0$ (bottom), $v_1 = 1$ (middle), and $v_1 = 2$ (top) for values of P increasing from -2 ($I = 0$) up to the value of the highest fitted polyad, that is, $P = 30$ ($I = 32$). For a given polyad $[v_1, P]$ the quantum energy levels all lie close in energy, as do also the energy values of the POs. Therefore, the full-scale plots displayed in the left part of this figure are difficult to interpret in detail. For clarity, the same information is plotted in the right part of the figure, but with an energy scale expanded around the energy of the stable PO with zero energy in the bend ($I = J$), which is labeled with an $[r]$ in the plots (the notation used to label the POs will be described in the next paragraph). For $v_1 = 0$ and below the bifurcation at $P = 12.30$, there exists only one extra PO in addition to $[r]$, a stable one labeled $[B]$; The $[r]$ - and $[B]$ -type POs form the backbones of the lowest and highest members of each polyad, respectively. Two other POs, labeled $[SN]$ and $[SN]$, are created at the tangent bifurcation. $[SN]$ denotes the stable PO, along which the wave functions of isomerization states are elongated, whereas $[SN]$ stands

for the unstable one. The agreement between classical POs and quantum nodal lines can be checked in Fig. 1, where the $[r]$, $[B]$, and $[SN]$ POs are plotted on top of the wave functions for polyad $[v_2, P]=[0,22]$. Of fundamental importance is the fact that the classically allowed region, that is, the values of E for which a classical trajectory exists, always lies between the two outermost POs for given values of v_1 and P . For example, for $v_1=0$ the energy of $[SN]$ crosses the energy of $[r]$ at $P=21.1$, so that the classically allowed region lies between $[r]$ and $[B]$ from $P=-2$ to $P=21.1$ and between $[SN]$ and $[B]$ for values of P larger than 21.1. Similarly, the quantum states always lie between the same outermost POs. For the sake of illustration, the quantum states for polyads $[v_1, P]=[0,14]$, $[0,22]$, $[0,30]$, $[1,24]$, and $[2,20]$ are shown as columns of small black dots in the figure. Notice that the tangent bifurcation always takes place close to the low-energy end of the classically allowed region (that is, correspondingly, to the low-energy end of the quantum polyad) and that the $[SN]$ stable PO then rapidly defines the low-energy border of the allowed region. *This is the reason why perturbations in the spectrum and isomerization states first appear near the low-energy end of the polyads, and not near the top, where they were first searched for by experimentalists.* We will return in more detail to this point in the next section.

The ratio $J/(P+2)$ for the POs is plotted in Fig. 4 for the same polyads as in Fig. 3, that is, for values of v_1 ranging from 0 to 2 and values of P from -2 to 30. Recall that J [Eq. (2.6)] remains constant for all of the POs discussed in this article^{9,34} and that a $J/(P+2)$ ratio close to zero means that the PO is an almost pure bending motion, whereas a ratio close to one describes a motion which remains in the neighborhood of the CP-stretch axis⁹ (stated in other words, ratios equal to 0 and 1 define the two poles of the polyad phase sphere). Figure 4 shows that the two stable POs, which exist for low values of P , have respective ratios of 0 and 1 for the lowest possible value of P , $P=-2$ ($I=0$). Therefore, in that limit, they correspond to pure bending and pure CP-stretching motions. This is why they are labeled as $[B]$ (B stands for bending) and $[r]$ (r is the Jacobi coordinate describing the length of the CP bond). Note that these labels are the same as the ones used in the classical study of the exact potential energy surfaces,^{6,7,11} whereas they describe subtly, but noticeably different objects: More precisely, the classical study is capable of finding one $[r]$ and one $[B]$ PO for each value of E and these trajectories are periodic in the six-dimensional phase space built on the three Jacobi coordinates r , R , and γ and their conjugate momenta; in contrast, the semiclassical study of the resonance effective Hamiltonian leads to one $[r]$ and one $[B]$ PO for each value of v_1 and P , and the trajectories are periodic in the four-dimensional space built on q_2 , q_3 , p_2 , and p_3 . Nonetheless, the same labels are used, because we think that this helps to make the link between the two kinds of studies. Returning to Fig. 4, it is seen that the $[r]$ PO remains a pure CP-stretching trajectory for all fitted polyads, while the $[B]$ PO acquires a substantial CP-stretch contribution as P increases, with a ratio $J/(P+2)$ close to 0.4 for the highest studied polyads. On the other hand, the stable $[SN]$ and unstable $[SN]$ POs are

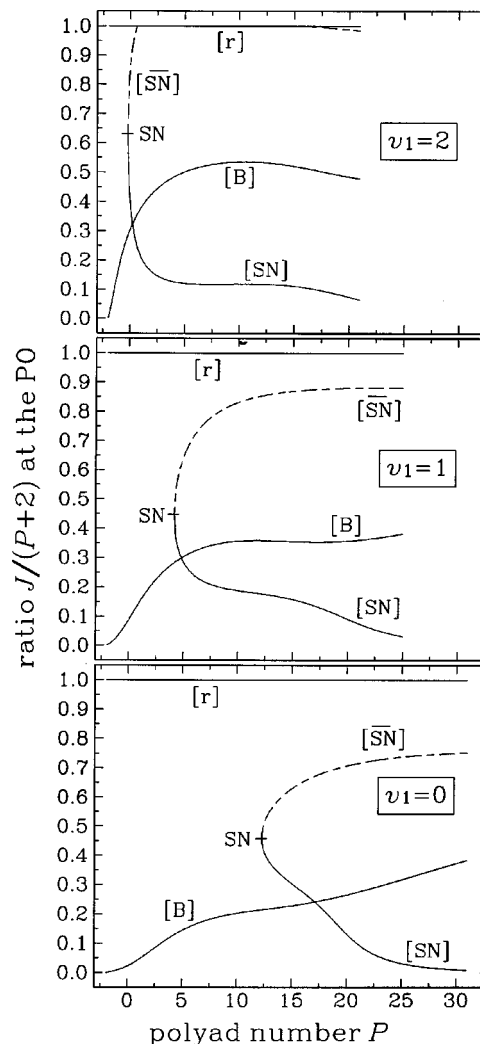


FIG. 4. Plot of the $J/(P+2)$ ratio at the periodic orbits of HCP as a function of the quantum polyad number P , for $v_1=0$ (bottom), $v_1=1$ (middle), and $v_1=2$ (top). $J/(P+2)$ is equal to zero for a pure bending motion and to one for a pure CP-stretching motion. Solid lines depict the $J/(P+2)$ ratio at the energy of the stable periodic orbits $[r]$, $[B]$, and $[SN]$ and the dashed line represents the $J/(P+2)$ ratio at the unstable periodic orbit $[SN]$. The cross labeled SN indicates the saddle-node (or tangent) bifurcation at which $[SN]$ and $[SN]$ are created simultaneously.

created with a very mixed character: At the bifurcation, $J/(P+2)$ is equal to 0.46, 0.45, and 0.63 for $v_1=0$, 1, and 2, respectively. As P increases, the CP-stretch contribution to $[SN]$ steadily decreases, while in contrast, the bending contribution diminishes for $[SN]$. Most importantly, high values of P and E are needed in order for $[SN]$ to become an almost pure bending motion and to consequently follow the minimum energy path to isomerization: indeed, the $J/(P+2)$ ratio becomes smaller than 0.1 only at $P=21.0$ and $E=12\,835\text{ cm}^{-1}$ above the quantum ground state for $v_1=0$, at $P=19.5$ and $E=14\,871\text{ cm}^{-1}$ for $v_1=1$ and at $P=17.0$ and $E=16\,289\text{ cm}^{-1}$ for $v_1=2$. *This slow evolution of the stable PO born at the bifurcation towards a pure bending motion is the reason why the new states only gradually arrange themselves along the isomerization pathway for the new surface, in contrast with what happens for the previous surface.*^{6,7,9}

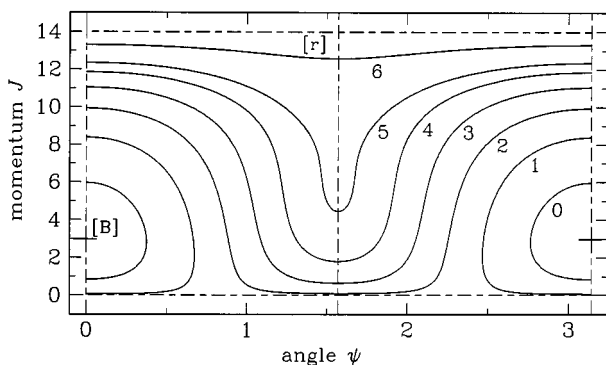
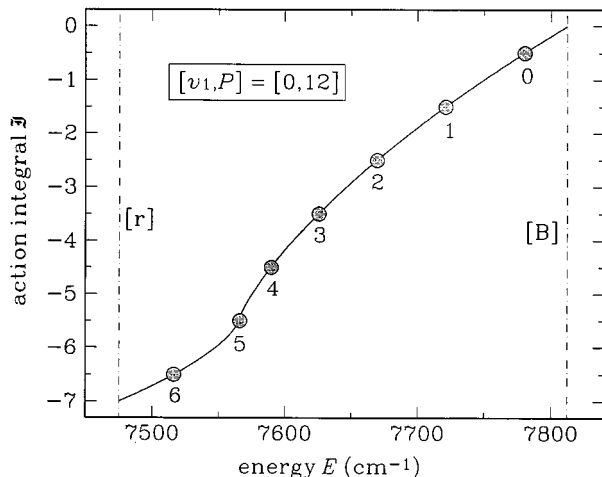
Quantizing trajectories for polyad $[v_1, P]=[0, 12]$ 

FIG. 5. The quantizing trajectories of HCP for polyad $[v_1, P]=[0, 12]$. The upper panel is a plot of the third action integral \mathcal{J} as a function of the energy E relative to the quantum ground state. Quantizing trajectories associated with quantum states, which correspond to half-integer values of \mathcal{J} , are shown as heavy black dots. The position i of the level inside the polyad is indicated close to each dot ($i=0$ for the highest level in the polyad, $i=P/2$ for the lowest one). The energies of the periodic orbits are indicated with vertical dot-dashed lines. The lower panel is a plot of the quantizing trajectories in the (J, ψ) surface of section. The position i of the corresponding level within the polyad is indicated close to each quantizing trajectory. The stable periodic orbit $[r]$ is shown as a line located at $J=P+2$, while the other periodic orbits appear as points in this surface of section.

V. QUANTIZING TRAJECTORIES AND THE INTERLEAVING OF NORMAL AND ISOMERIZATION STATES

Quantizing trajectories are studied in this section, in order to understand the interleaving of isomerization and normal states at the bottom of Fermi polyads.

Plots of the third action integral \mathcal{J} as a function of energy are shown in the upper panels of Figs. 5 and 6 for the polyads $[v_1, P]=[0, 12]$ and $[v_1, P]=[0, 22]$, the former polyad being located below the bifurcation for $v_1=0$ and the later one above it. Notice that these plots comprise either one (before bifurcation) or three branches (after bifurcation). Each branch starts and stops at one of the POs, either stable or unstable (the energy values for these POs are indicated with vertical dot-dashed lines in the upper panels of Figs. 5 and 6). The quantizing trajectories associated with the quantum states correspond to half-integer values of \mathcal{J} and are

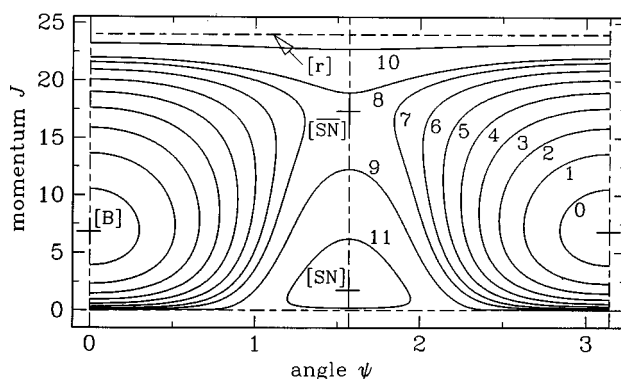
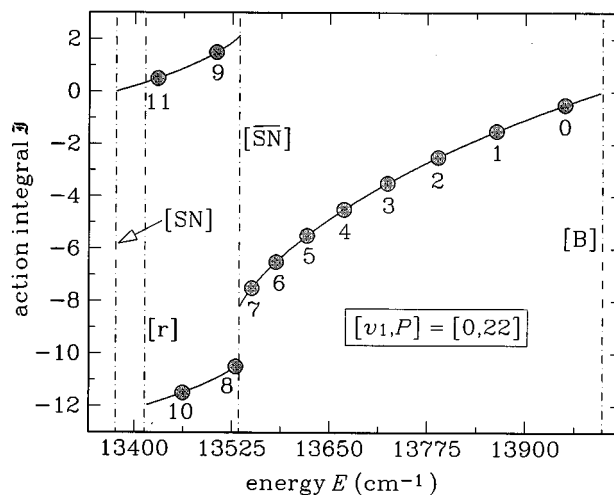
Quantizing trajectories for polyad $[v_1, P]=[0, 22]$ 

FIG. 6. Same as Fig. 5, but for polyad $[v_1, P]=[0, 22]$.

represented by heavy dots in these panels. The number close to each dot is the position i of the level inside the polyad. Incidentally, it is noted that the agreement between the energies of quantum states and quantizing trajectories is excellent, the largest error for polyad $[v_1, P]=[0, 22]$ being smaller than 1.3 cm^{-1} . The quantizing trajectories are also plotted in the (J, ψ) surface of section in the lower panels of Figs. 5 and 6. These plots are symmetric with respect to the $\psi=0$ and $\psi=\pi/2$ axes and periodic with a period equal to π . In the (J, ψ) surface, the $[B]$, $[SN]$, and $[\overline{SN}]$ POs only appear as points (because of the periodicity, $[B]$ appears as one point on both the $\psi=0$ and $\psi=\pi$ axes), while the $[r]$ PO appears as a horizontal line located at $J=I=P+2$. Each solid line in these plots further represents one quantizing trajectory, that is, one quantum state, except for the trajectories looping around $[B]$, which appear as two lines symmetric with respect to $\psi=\pi$. The position i of the level in the polyad is indicated close to each quantizing trajectory, to show its identification clearly. What happens as P increases and approaches from below the value where the bifurcation occurs, is that a point with higher and higher derivative (almost vertical tangent) develops in the plot of $\mathcal{J}=\mathcal{J}(E)$. Such a point is clearly seen close to $i=5$ in the upper panel of Fig. 5. At the bifurcation, the tangent becomes exactly vertical and the plot $\mathcal{J}=\mathcal{J}(E)$ splits into two segments at this

point. These are the two branches, which appear at negative values of \mathcal{J} in the upper panel of Fig. 6. The gap between the two segments is vanishingly small at the bifurcation but increases substantially as P becomes larger than the value at the bifurcation. It should, however, be realized, that this splitting into two branches does not result in the appearance of a new kind of motion: Indeed, it is clearly seen in the lower panels of Figs. 5 and 6 that the quantizing trajectories with $i=0$ and $i=1$ for $P=12$ are topologically equivalent to the trajectories with $i=0$ to $i=7$ for $P=22$. Similarly, the quantizing trajectories with $i=2$ to $i=6$ for $P=12$ are equivalent to the trajectories with $i=8$ and $i=10$ for $P=22$. In contrast, above the bifurcation a third branch develops between the energies of the two POs which appear at the bifurcation, namely $[SN]$ and $[\overline{SN}]$. At the bifurcation these two POs are energetically degenerate, but then they separate widely as P increases, and $[SN]$ rapidly defines the lower border of the classically allowed region. Similarly, $[SN]$ and $[\overline{SN}]$ are created at the same point on the $\psi=\pi/2$ axis, but then separate further and further as P increases. As can be verified in the lower panel of Fig. 6, the quantizing trajectories located on this branch with positive values of \mathcal{J} do represent a new kind of motion, since they either loop around the $[SN]$ PO (as for $i=11$) or spend most of the time close to the $J=0$ axis (as for $i=9$). Not surprisingly, these quantizing trajectories with a new, predominantly bending type of motion are those, which are associated with the quantum isomerization states (see Fig. 1).

We are now in the position to discuss two further quantum observations, namely the first appearance of isomerization states at P and E values substantially larger than the bifurcation values and, more interestingly, the interleaving of normal states and isomerization states near the low-energy end of the polyads. For that purpose, it should be emphasized that the EBK quantization rule, which states that quantizing trajectories have half-integer values of \mathcal{J} , applies to each of the branches when more than one of them is observed in the plot of $\mathcal{J}=\mathcal{J}(E)$. Now, the branch supporting the new, bending type of trajectories starts at $\mathcal{J}=0$ at the bifurcation and develops to higher and higher positive values of \mathcal{J} as P increases. Clearly, *isomerization states appear for the first (even) value of P , for which the branch extends beyond $\mathcal{J}=1/2$* . This is the reason why, for $v_1=0$, the first isomerization state is observed in polyad $P=16$, whereas it could have been expected in polyad $P=14$ (recall that $P=12.30$ at the bifurcation). Moreover, as is confirmed in the lower panel of Fig. 6, there are two coexisting branches in the plot of $\mathcal{J}=\mathcal{J}(E)$ in the energy range between $[r]$ or $[SN]$ and $[\overline{SN}]$. In other words, for each value of the energy lying between the $[\overline{SN}]$ and $[r]$ or $[SN]$ limits there exist two trajectories, one with predominant bending behavior and another with predominant CP-stretching behavior. *If this energy region is sufficiently broad, so that at least one quantizing trajectory exists on each branch within the range, then the inevitable result is an interleaving of normal and isomerization states*, the specific ordering depending on which branch crosses a half-integer value of \mathcal{J} at which energy. On the other hand, looking back at the upper right plot in Fig. 3, one notices that, for $v_1=2$, the $[r]$ and $[SN]$ POs remain

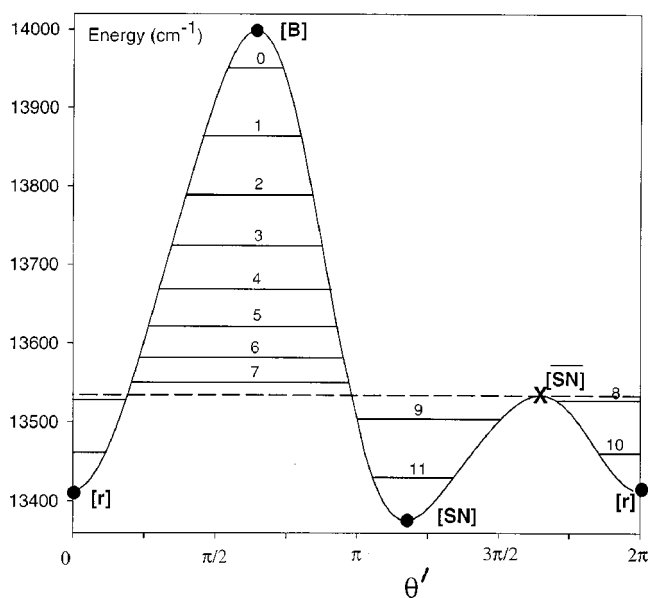
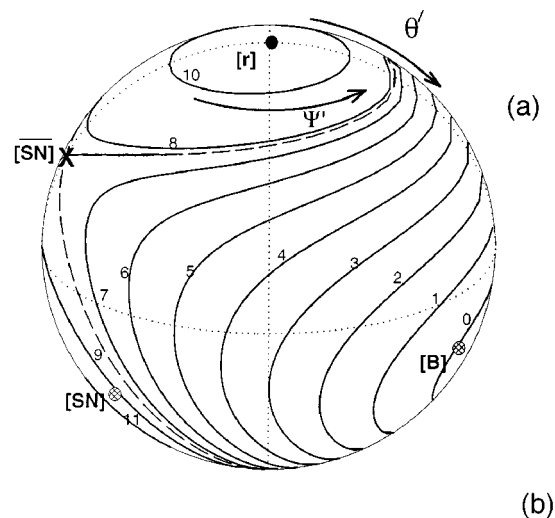


FIG. 7. (a) Polyad phase sphere representation of the $P=22$ polyad. Each energy level obtained from the diagonalization of the Fermi resonance effective Hamiltonian corresponds to a trajectory on the sphere. The phase space portraits of Figs. 5 and 6 are analogous to Mercator projections of the phase sphere. However, the trajectories in Figs. 5 and 6 differ in that they correspond to energy levels obtained from semiclassical quantization, rather than direct matrix diagonalization; see text. Stable POs are indicated by circles (the hatched circles represent points on the back of the sphere); the X indicates an unstable PO. The dashed line is the separatrix. (b) Pseudopotential obtained by plotting the energy as a function of the angle θ' of the great circle on the sphere on which all the fixed points (or POs in the full phase space) lie. All of the fixed points correspond to extrema of the pseudopotential.

almost degenerate (from the energetic point of view) for all possible values of P . *This is the reason why no interleaving of normal and isomerization states is observed in the quantum spectrum for $v_1=2$: the energy region in which the two branches coexist is too narrow.*

It is useful to relate the phase space portraits of Figs. 5 and 6 to the polyad phase sphere representation of Kellman and co-workers.^{17-19,21-24} Figure 7(a) shows the phase sphere representation for the $P=22$ polyad, the phase space portrait of which was shown as Fig. 6(b). From the phase sphere point of view, the phase space portraits are Mercator

projections of the phase sphere, with relations to the polyad numbers and angles as follows:

$$I' = \frac{1}{4},$$

$$\theta' = \arccos\left(\frac{2J-I}{I}\right), \quad (5.1)$$

$$\psi' = \frac{\psi}{2},$$

where I' , θ' , and ψ' are the radial coordinates defining each point on the sphere, and I , J , ψ have been defined in Eq. (2.6).

In the phase sphere representation, constraints on the possible combinations of POs arise from the Poincaré index theorem, which states: If an index is associated with each PO according to its stability:

$$\text{Index} = \begin{cases} 1 & \text{if stable} \\ -1 & \text{if unstable,} \\ 0 & \text{if it is a cusp,} \end{cases} \quad (5.2)$$

then the sum over all POs of these indices is determined by the topology of the phase space alone. Specifically, for a 2D (two-dimensional) sphere we have:

$$\sum \text{Indices} = 2. \quad (5.3)$$

The two simplest kinds of bifurcation that satisfy the index theorem are the ‘‘cusp type,’’ at which a cusp PO first appears^{17,22,23} and the ‘‘SN type,’’ in which a pair of stable–unstable POs are created. In this paper, only the SN bifurcation has been encountered, while the cusp type bifurcation has been observed in other systems, notably in substituted methane molecules^{22,23} and HOCl.³⁴ In the phase sphere representation, it turns out that all the POs of the Fermi resonance Hamiltonian lie on a great circle passing through the north ($\psi' = 0$) and south ($\psi' = \pi$) poles of the sphere. On the reduced one-dimensional subspace comprising the great circle, the POs manifest themselves as extrema or inflection points of the energy. Hence, they can be conveniently identified by examining the ‘‘pseudopotential’’ in which the energy on the phase sphere is plotted vs the angle along the great circle.³⁶ The pseudopotential for the $P=22$ polyad sphere is sketched in Fig. 7(b), which illustrates how all of the fixed points in Fig. 6(b) and 7(a) lie at extrema.

VI. UNSTABLE POs AND PATTERNS IN THE GAP BETWEEN NEIGHBORING LEVELS

In Sec. IV, the shapes of quantum wave functions have been interpreted in terms of the properties of the *stable* POs of the classical Hamiltonian. In this section, patterns of the energy spacing between adjacent levels within a quantum polyad will instead be connected to the *unstable* classical POs.

The unstable POs are not only dynamically important in themselves, but they also define the structures called separatrices, which divide the classical phase space into dynamically

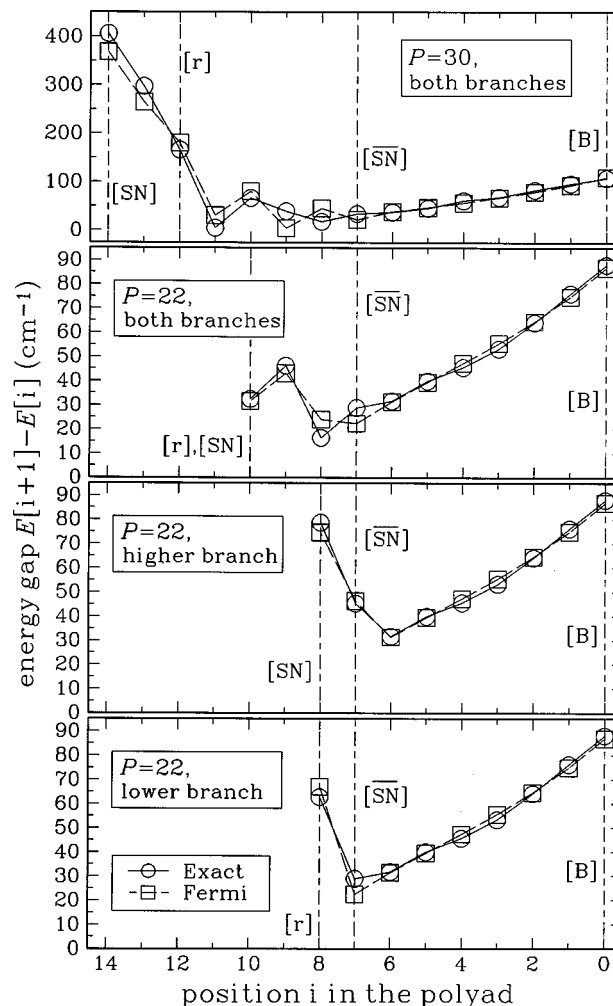


FIG. 8. Plot of the energy gap between levels i and $i+1$ as a function of i for polyads $[v_1, P] = [0, 22]$ ((b), (c), and (d)) and $[v_1, P] = [0, 30]$ (a) for the levels of the *ab initio* PES (circles) (Refs. 10 and 11) and the Fermi resonance Hamiltonian (squares). The dot–dashed vertical lines indicate the positions of the classical periodic orbits. See the text for a discussion of the three plots for $P=22$.

distinct regions. The energy spacings are therefore an important means by which to decode information about the molecular dynamics from the spectrum. These kinds of patterns have been considered by Svitak *et al.*¹⁷ for the most elementary version of the Fermi resonance Hamiltonian, i.e., one which differs from the present study in that it includes only second-order terms in the Dunham expansion for the zero-order part of the Hamiltonian. The simplest of these patterns is a minimum or ‘‘dip’’ in the spacings of adjacent levels in a polyad, due to the presence of a classical separatrix.

A separatrix is a phase space structure that contains an unstable PO. The simple minimum in the level spacings is associated, in the work of Svitak *et al.*,¹⁷ with an unstable PO, which in the reduced phase of the sphere appears as a fixed point, lying at a cusp on the separatrix. (In Ref. 17, the dip occurs in the region classified as ‘‘zone II dynamics’’ by Xiao and Kellman^{23,24}). More complicated phase space structures, e.g., those formed after a SN bifurcation, which involve more than one PO, can give rise to more complex

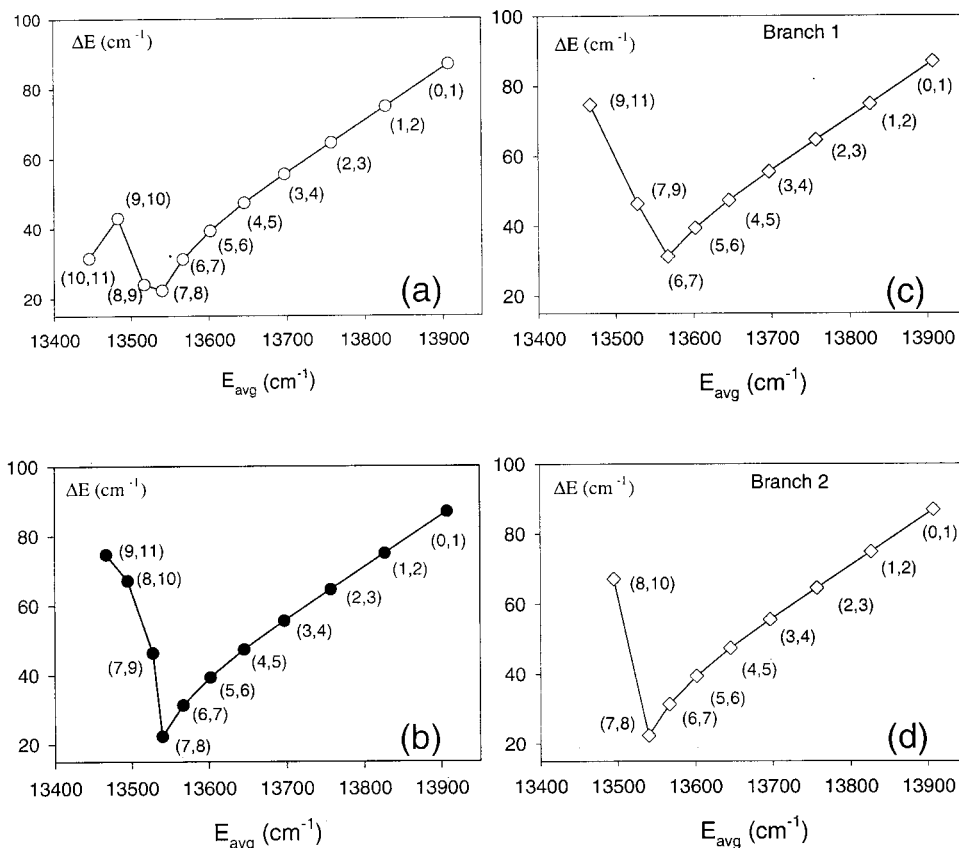


FIG. 9. Energy level patterns of the $P=22$ polyad, plotted according to the procedure of Svitak *et al.* (Ref. 36) compared with the similar procedure of Fig. 8. The energy spacing between appropriately chosen pairs of levels is plotted as a function of the average energy of the two levels in the pair. (a) shows the levels chosen in order of energy, resulting in a “zig-zag” or “interleaving fan;” (b) shows the levels chosen after sorting by the assignment procedure of Xiao and Kellman (Refs. 23 and 24) (c) and (d) show the levels sorted by the slightly different procedure of Fig. 8. In (b), (c), and (d) the “zig-zag” is replaced by a single dip, indicating the presence and location of the separatrix.

spectral patterns,¹⁷ a fact of which we will make use shortly. In light of Ref. 17, Ishikawa *et al.*⁵ noted the presence of a minimum in the energy level spacings of the complete polyads resulting from a fit of their incomplete experimental data for HCP to a version of the Fermi resonance Hamiltonian. Here we will consider the presence and meaning of such patterns in the refined version of the spectroscopic Hamiltonian we have developed in this paper.

The link between the classical phase space structure and quantum spectral patterns arises from the following considerations: (i) The classical frequency ω^* associated with the third action integral \mathcal{J} goes logarithmically to zero at the unstable $[\overline{SN}]$ PO;¹⁵ (ii) the slope of $\mathcal{J}=\mathcal{J}(E)$ is just $1/\omega^*$; (iii) quantum states are associated through the EBK quantization rule with equally spaced, half-integer values of \mathcal{J} . Therefore, the energy gap between two neighboring levels within a polyad decreases as these levels approach the unstable PO. Consequently, if a single branch exists in the plot of $\mathcal{J}=\mathcal{J}(E)$ on both sides of $[\overline{SN}]$, then the unstable PO is responsible for a minimum in the spacings between adjacent levels. This phenomenon is the spectral minimum noted by Svitak *et al.*¹⁷ This is precisely what happens in the spectrum based on the fit by Ishikawa *et al.* of an effective Hamiltonian model to experimental data.⁵ As noted above, in the present model for HCP, the spectral situation is more complex above the SN bifurcation. Two branches coexist in the

plot of \mathcal{J} on the low-energy side of $[\overline{SN}]$, and more precisely between $[\overline{SN}]$ and $[r]$ (if $[r]$ has an energy greater than $[\overline{SN}]$) or $[\overline{SN}]$ and $[\overline{SN}]$ (if $[\overline{SN}]$ has an energy greater than $[r]$). A similar situation was considered by Svitak *et al.*¹⁷ for the case of Xiao and Kellman’s^{23,24} “zone III” dynamics. If one considers the adjacent level separations along each branch separately, then the minimum spacing is still clearly evident. This is illustrated in Fig. 8: The bottom plot shows the spacings between adjacent levels of polyad $P=22$ when only the lower branch (negative values of \mathcal{J}) is considered on the low-energy side of $[\overline{SN}]$. In other words, the polyad is treated as if it contains levels $i=10$ and all the levels from $i=8$ down to $i=0$, the levels $i=9$ and $i=11$ (which belong to the higher branch) being excluded. The minimum in the level spacing is quite clear and occurs at $[\overline{SN}]$. Similarly, the penultimate plot in Fig. 8 displays the energy spacings between the levels of polyad $P=22$, when only the higher branch is considered on the low-energy side of $[\overline{SN}]$, that is, when the levels $i=8$ and $i=10$ are excluded. Here again, the minimum is clear. The point is that one must consider the two branches simultaneously because both are present in the spectrum. Since these two branches are parallel (because ω^* is the same for the two branches¹⁵), this results in a zig-zag in the plot of the adjacent level spacings, as can be seen in the second highest plot of Fig. 8. This zig-zag is simply due

to the fact that two families of level spacings $E[i+1] - E[i]$ coexist: The first family is associated with odd values of i and the second one with even values of i . Since the zig-zag behavior takes place over the entire energy range, where two trajectories with the same value of energy coexist, a simple monotonic decrease of the level spacings can only be observed between the two stable $[SN]$ and $[r]$ POs. The example for polyad $P=30$ is illustrated by the upper plot of Fig. 8.

It is also useful to consider this pattern from the related viewpoint of the work of Svitak *et al.*¹⁷ and the pseudopotential on the great circle of the polyad sphere. In Ref. 17, the zig-zag pattern was described as an “interleaving fan” which was rearranged into a single “minimum” pattern, using an assignment method proposed by Xiao and Kellman.²⁴ That method of sorting the energy level can be understood with reference to the pseudopotential in Fig. 7(b). The zig-zag pattern, shown in Fig. 9(a), is sorted into a single minimum, shown in Fig. 9(b), obtained by taking energy separations only between levels which belong to the same well of the pseudopotential. An essentially equivalent procedure is to sort the levels in Fig. 9(b) into two sets, one for each of the wells labeled $[r]$ and $[SN]$ in the Fig. 7(b) pseudopotential. Figures 9(c) and 9(d) are obtained in this way. They are obviously completely equivalent to the two bottom plots in Fig. 8.

VII. CONCLUSION

In the present article we have demonstrated that most of the features, which were empirically found in the vibrational wave functions and energy levels for an *ab initio* PES of almost spectroscopic accuracy, can be reproduced by an effective resonance Hamiltonian. More important than only reproducing exact quantum calculations, however, the study of the resonance Hamiltonian enables these observations to be interpreted in terms of classical periodic orbits and quantizing trajectories to an extent that is exceedingly difficult to achieve from the study of the exact Hamiltonian alone.

Since the discovery of isomerization states in HCP,^{6,7} other molecules were found to display strong perturbations associated with a classical bifurcation, like HOCl,^{34,37} C₂H₂³⁵ and, more recently, DCP.³⁸ At the present time, however, HCP remains unique, because it is the only molecule for which perturbations due to a reaction pathway have been detected experimentally.¹⁻⁵ Due to the rapid development of experimental tools and computer capabilities, it is most probable that many other molecules will be shown to display the same kind of features in the near future. It is hoped that the work on HCP will convince people working in that field that it is only through the collecting of the different pieces mentioned in the introduction, namely, experimental data, exact quantum calculation on a precise *ab initio* PES, classical analysis of this PES, and semiclassical study of an effective Hamiltonian, that a most precise and global understanding of the dynamics of these molecules can be achieved.

ACKNOWLEDGMENTS

R.W.F. is grateful for an AFOSR Grant No. F49620-97-1-0040. C.B. and R.S. acknowledge financial support by the Deutsche Forschungsgemeinschaft through the Sonderforschungsbereich 357 “Molekulare Mechanismen Unimolekularer Reaktionen” and the Fonds der Chemischen Industrie.

- ¹K. K. Lehmann, S. C. Ross, and L. L. Lohr, *J. Chem. Phys.* **82**, 4460 (1985).
- ²Y. T. Chen, D. M. Watt, R. W. Field, and K. K. Lehmann, *J. Chem. Phys.* **93**, 2149 (1990).
- ³H. Ishikawa, Y. T. Chen, Y. Ohshima, J. Wang, and R. W. Field, *J. Chem. Phys.* **105**, 7383 (1996).
- ⁴H. Ishikawa, C. Nagao, N. Mikami, and R. W. Field, *J. Chem. Phys.* **106**, 2980 (1997).
- ⁵H. Ishikawa, C. Nagao, N. Mikami, and R. W. Field, *J. Chem. Phys.* **109**, 492 (1998).
- ⁶S. C. Farantos, H. M. Keller, R. Schinke, K. Yamashita, and K. Morokuma, *J. Chem. Phys.* **104**, 10055 (1996).
- ⁷C. Beck, H. M. Keller, S. Yu. Grebenshchikov, R. Schinke, S. C. Farantos, K. Yamashita, and K. Morokuma, *J. Chem. Phys.* **107**, 9818 (1997).
- ⁸M. Joyeux, *J. Chem. Phys.* **109**, 2111 (1998).
- ⁹M. Joyeux, S. Yu. Grebenshchikov, and R. Schinke, *J. Chem. Phys.* **109**, 8342 (1998).
- ¹⁰C. Beck, R. Schinke, and J. Koput (to be published).
- ¹¹H. Ishikawa, R. W. Field, S. C. Farantos, M. Joyeux, J. Koput, C. Beck, and R. Schinke, *Annu. Rev. Phys. Chem.* **50**, 443 (1999).
- ¹²M. Joyeux, *Chem. Phys.* **221**, 269 (1997).
- ¹³M. Joyeux, *Chem. Phys.* **221**, 287 (1997).
- ¹⁴M. Joyeux, *Chem. Phys.* **185**, 263 (1994).
- ¹⁵M. Joyeux, *Chem. Phys.* **203**, 281 (1996).
- ¹⁶V. P. Maslov and M. V. Fedoriuk, *Semiclassical Approximations in Quantum Mechanics* (Deidel, Dordrecht, 1981).
- ¹⁷J. Svitak, Z. Li, J. Rose, and M. E. Kellman, *J. Chem. Phys.* **102**, 4340 (1995).
- ¹⁸M. E. Kellman, in *Molecular Dynamics and Spectroscopy by Stimulated Emission Pumping*, edited by H.-L. Dai and R. W. Field (World Scientific, Singapore, 1995), pp. 943-997.
- ¹⁹M. E. Kellman, *Annu. Rev. Phys. Chem.* **46**, 395 (1995).
- ²⁰M. E. Kellman and E. D. Lynch, *J. Chem. Phys.* **85**, 7216 (1986).
- ²¹L. Xiao and M. E. Kellman, *J. Chem. Phys.* **90**, 6086 (1989).
- ²²Z. Li, L. Xiao, and M. E. Kellman, *J. Chem. Phys.* **92**, 2251 (1990).
- ²³L. Xiao and M. E. Kellman, *J. Chem. Phys.* **93**, 5805 (1990).
- ²⁴L. Xiao and M. E. Kellman, *J. Chem. Phys.* **93**, 5821 (1990).
- ²⁵M. C. Gutzwiller, *J. Math. Phys.* **8**, 1979 (1967).
- ²⁶M. C. Gutzwiller, *J. Math. Phys.* **12**, 343 (1971).
- ²⁷M. C. Gutzwiller, *Chaos in Classical and Quantum Mechanics* (Springer Verlag, Berlin, 1990).
- ²⁸E. J. Heller, *Phys. Rev. Lett.* **53**, 1515 (1984).
- ²⁹P. O'Connor, J. Gehlen, and E. J. Heller, *Phys. Rev. Lett.* **58**, 1296 (1987).
- ³⁰J. M. G. Llorente and E. Pollak, *Annu. Rev. Phys. Chem.* **43**, 91 (1992).
- ³¹H. S. Taylor, in *Molecular Dynamics and Spectroscopy by Stimulated Emission Pumping*, edited by H.-L. Dai and R. W. Field (World Scientific, Singapore, 1995), p. 891.
- ³²R. Schinke, *Photodissociation Dynamics* (Cambridge University Press, Cambridge, 1993).
- ³³S. C. Farantos, *Int. Rev. Phys. Chem.* **15**, 345 (1996).
- ³⁴R. Jost, M. Joyeux, S. Skokov, and J. Bowman, *J. Chem. Phys.* **111**, 6807 (1999).
- ³⁵M. P. Jacobson, C. Jung, H. S. Taylor, and R. W. Field, *J. Chem. Phys.* **111**, 600 (1999).
- ³⁶J. Svitak, thesis.
- ³⁷J. Weiss, J. Hauschildt, S. Yu. Grebenshchikov, R. Düren, R. Schinke, J. Koput, S. Stamatiadis, and S. C. Farantos, *J. Chem. Phys.* **112**, 77 (2000).
- ³⁸J. Bredenbeck, C. Beck, R. Schinke, J. Koput, S. Stamatiadis, S. C. Farantos, and M. Joyeux, *J. Chem. Phys.* (to be published).